

A Contribution of Image Processing to the Diagnosis of Diabetic Retinopathy—Detection of Exudates in Color Fundus Images of the Human Retina

Thomas Walter*, Jean-Claude Klein, Pascale Massin, and Ali Erginay

Abstract—In the framework of computer assisted diagnosis of diabetic retinopathy, a new algorithm for detection of exudates is presented and discussed. The presence of exudates within the macular region is a main hallmark of diabetic macular edema and allows its detection with a high sensitivity. Hence, detection of exudates is an important diagnostic task, in which computer assistance may play a major role. Exudates are found using their high grey level variation, and their contours are determined by means of morphological reconstruction techniques. The detection of the optic disc is indispensable for this approach. We detect the optic disc by means of morphological filtering techniques and the watershed transformation. The algorithm has been tested on a small image data base and compared with the performance of a human grader. As a result, we obtain a mean sensitivity of 92.8% and a mean predictive value of 92.4%. Robustness with respect to changes of the parameters of the algorithm has been evaluated.

Index Terms—Diabetic retinopathy, exudates, image processing, mathematical morphology, optic disc, papilla.

I. INTRODUCTION

DIABETIC retinopathy is a severe and widely spread eye disease. It is the commonest cause of legal blindness in the working-age population of developed countries. That is the reason for the intensified effort that has been undertaken in the last years in developing tools to assist in the diagnosis of diabetic retinopathy.

The first part of this introductory section is dedicated to a discussion of the ways in which image processing can contribute to the diagnosis of diabetic retinopathy. The second part gives a short introduction to the morphological operators that are used in this paper. In the next two sections, we give examples of algorithms that can be integrated in a tool for diagnosis of diabetic retinopathy: The detection of the optic disc (papilla) and the detection of retinal exudates. Both algorithms are validated on a small image data base. Finally, we conclude and give some perspectives for future work.

Manuscript received November 5, 2001; revised July 16, 2002. Asterisk indicates corresponding author.

*T. Walter is with the Center of Mathematical Morphology, Paris School of Mines, 35 Rue. St. Honore, 77305 Fontainebleau cedex, France (e-mail: walter@cmm.ensmp.fr).

J.-C. Klein is with the Center of Mathematical Morphology, Paris School of Mines, 77305 Fontainebleau cedex, France.

P. Massin and A. Erginay are with Hôpital Lariboisière, Service Ophtalmologie, 75475 Paris cedex 10, France.

Digital Object Identifier 10.1109/TMI.2002.806290

A. Contribution of Image Analysis to the Diagnosis of Diabetic Retinopathy

The contribution of image processing to the diagnosis of diabetic retinopathy may be divided into the following three groups:

- 1) image enhancement;
- 2) mass screening;
- 3) monitoring of the disease.

Image Enhancement: Images taken at standard examinations are often noisy and poorly contrasted. Over and above that, illumination is not uniform. Techniques improving contrast and sharpness and reducing noise are therefore required

- as an aid for human interpretation of the fundus images;
- as a first step toward automatic analysis of the fundus images.

Standard contrast stretching techniques have been applied by [1], [2], and [3]; methods that allow enhancement of certain features (e.g., only microaneurysms) have been proposed in [4]; image restoration techniques for images of very poor quality (e.g., due to cataracts) have been applied in [5] and [6].

Mass Screening: Computer-assisted mass screening for diagnosis of diabetic retinopathy is certainly the most important task to which image processing can contribute.

Although the mechanisms for diabetic retinopathy are not fully understood, its progress can be inhibited by early diagnosis and treatment. However, as vision normally alters only in the later stages of the disease, many patients remain undiagnosed in the earlier stages of the disease, when treatment would be the most efficient. Hence, mass screening of all diabetic patients (even without vision impairment) would help to diagnose this disease early enough for an optimal treatment. An automated or semiautomated computer-assisted diagnosis could bring the following advantages:

- diminution of the necessary resources in terms of specialists;
- diminution of the examination time.

The tasks for image processing may be divided into the following.

- Automatic detection of pathologies: microaneurysms ([7]–[11]), hard exudates and cotton wool spots [2], [11]–[13], hemorrhages, and edema.

- Automatic detection of features of the retina: The vascular tree [1], [7], [14]–[19], and the optic disc ([14], [17], [1], [20], [19]). Feature detection is necessary for the identification of false positives in the pathology detection and for the classification of the pathologies in accordance with their severity.
- Measurements on the detected pathologies that are difficult or too time consuming to be done manually.

Monitoring: In order to assess the evolution of the disease, physicians have to compare images taken at different medical examinations. This allows one to

- evaluate for each patient the efficiency of the ophthalmologic and diabetic treatments;
- evaluate the efficiency of new therapeutics in a population of patients;
- observe the development of single lesions (for example in order to study the turn-over effect of microaneurysms).

However, the comparison of images taken at different moments is a very time-consuming task and open to human error due to the distortions between images that make superposition very difficult, and due to the large number of lesions that have to be compared. A computer assisted approach is needed. In addition to automatic detection of pathologies, such a tool needs a robust feature-based registration algorithm.

Registration algorithms for retinal images have been proposed in [17], [10], and [21].

B. Some Morphological Operators

In this section, we briefly define the basic morphological operators used in this paper (for a comprehensive introduction, see [22]; for an exhaustive presentation, see [23]).

Let \mathcal{D}_f be a subset of \mathbb{Z}^2 and $T = \{t_{\min}, \dots, t_{\max}\}$ be an ordered set of grey-levels. A grey-level image f can then be defined as a function $f : \mathcal{D}_f \subset \mathbb{Z}^2 \rightarrow T = \{t_{\min}, \dots, t_{\max}\}$. Furthermore, let B be a subset of \mathbb{Z}^2 and $s \in \mathbb{N}$ a scaling factor, we can write the basic morphological operations as follows.

- Erosion: $[\varepsilon^{(sB)}(f)](x) = \min_{b \in sB} f(x + b)$.
- Dilation: $[\delta^{(sB)}(f)](x) = \max_{b \in sB} f(x + b)$.
- Opening: $\gamma^{(sB)}(f) = \delta^{(sB)}[\varepsilon^{(sB)}(f)]$.
- Closing: $\phi^{(sB)}(f) = \varepsilon^{(sB)}[\delta^{(sB)}(f)]$.

We call sB structuring element B of size s . Furthermore, we define the geodesic transformations of an image f (marker) and a second image g (mask)

- $\varepsilon_g^{(n)}(f) = \varepsilon_g^{(1)} \varepsilon_g^{(n-1)}(f)$ with $\varepsilon_g^{(1)}(f) = \varepsilon^{(B)}(f) \vee g$;
- $\delta_g^{(n)}(f) = \delta_g^{(1)} \delta_g^{(n-1)}(f)$ with $\delta_g^{(1)}(f) = \delta^{(B)}(f) \wedge g$;
- $R_g(f) = \delta_g^{(i)}(f)$ with $\delta_g^{(i)}(f) = \delta_g^{(i+1)}(f)$;
- $R_g^*(f) = \varepsilon_g^{(i)}(f)$ with $\varepsilon_g^{(i)}(f) = \varepsilon_g^{(i+1)}(f)$;

where $\varepsilon_g^{(n)}(f)$, $\delta_g^{(n)}(f)$, $R_g(f)$ and $R_g^*(f)$ are called geodesic erosion, geodesic dilation, reconstruction by dilation, and reconstruction by erosion, respectively.

Furthermore, we shall make use of the watershed transformation (see [24]), for which we do not give a mathematical definition here.

II. DETECTION OF THE OPTIC DISC

A. Outlines

The detection of the optic disc in the human retina is a very important task. It is indispensable for our approach to detection of exudates, because the optic disc has similar attributes in terms of brightness, color and contrast, and we shall make use of these characteristics for the detection of exudates. Over and above that, the optic disc can be seen as a landmark and it can be used for a coarse registration of retinal images in order to reduce the search space for a finer one. Furthermore, its detection is a first step in understanding ocular fundus images: The diameter delivers a calibration of the measurements that are done [13], and it determines approximately the localization of the macula [14], the center of vision, which is of great importance as lesions in the macular region affect vision immediately.

B. Properties of the Optic Disc

The optic disc is the entrance of the vessels and the optic nerve into the retina. It appears in color fundus images as a bright yellowish or white region. Its shape is more or less circular, interrupted by the outgoing vessels. Sometimes the optic disc has the form of an ellipse because of a nonnegligible angle between image plane and object plane. The size varies from patient to patient; its diameter lies between 40 and 60 pixels in 640×480 color photographs.

C. State of the Art

In [1], the optic disc is localized exploiting its high grey level variation. This approach has been shown to work well, if there are no or only few pathologies like exudates that also appear very bright and are also well contrasted. No method is proposed for the detection of the contours.

In [15], an area threshold is used to localize the optic disc. The contours are detected by means of the Hough transform, i.e., the gradient of the image is calculated, and the best fitting circle is determined. This approach is quite time consuming and it relies on conditions about the shape of the optic disc that are not always met. Sometimes, the optic disc is even not visible entirely in the image plane, and so the shape is far from being circular or even elliptic.

Also, in [17], the Hough transform is used to detect the contours of the optic disc in infrared and argon-blue images. Despite of some improvements, problems have been stated if the optic disc does not meet the shape conditions (e.g., if it lies on the border of the image) or if contrast is very low.

In [14], the optic disc is localized by backtracing the vessels to their origin. This is certainly one of the safest ways to localize the optic disc, but it has to rely on vessel detection. It is desirable to separate segmentation tasks in order to avoid an accumulation of segmentation errors and to save computational time (the detection of the vascular tree is particularly time consuming).

In [20], morphological filtering techniques and active contours are used to find the boundary of the optic disc, in [19] an area threshold is used to localize the optic disc and the watershed transformation to find its contours.

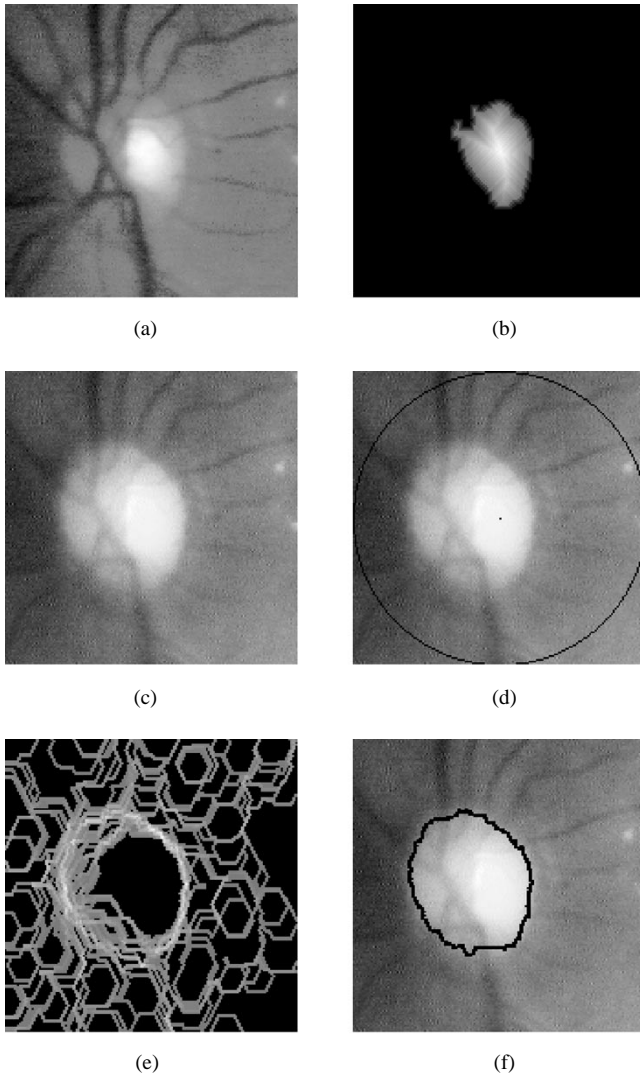


Fig. 1. The detection of the optic disc. (a) Luminance channel, (b) distance image of the biggest particle, (c) red channel, (d) red channel with imposed marker, (e) morphological gradient, and (f) result of segmentation.

D. Approach Based on the Watershed Transformation

1) *Color Space*: Having compared several color spaces, we found the contours of the optic disc to appear most continuous and most contrasted against the background in the red channel f_r of the *RGB* color space. As this channel has a very small dynamic range, and as we know that the optic disc belongs to the brightest parts of the color image, it is more reliable to work on the luminance channel f_l of the *HLS* color space in order to localize the optic disc and on f_r to find its contours [compare the Fig. 1(a) and (c)].

2) *Localizing the Optic Disc*: As in [1], we want to use local grey level variation for finding the locus of the optic disc. As the optic disc is a bright pattern, and as the vessels appear dark, the grey level variation in the papillary region is higher than in any other part of the image. Unfortunately, this is only true, if there are no exudates on a dark background. We apply, therefore, a shade-correction operator in order to remove slow background variations, i.e., we calculate $l_1 = f_l - I(f_l) + k$ where k is a positive constant and $I(f_l)$ is an approximation of the slow variations of f_l , that has been computed by a large median or mean

filter, by homomorphic filtering or by alternating sequential filters. In order to avoid artifacts at the borders of bright regions, we use alternating sequential filters to calculate the background approximation

$$I(f_l) = ASF(f_l) = \phi^{(nB)}(\dots(\gamma^{(2B)}(\phi^{(B)}(\gamma^{(B)}(f_l))))\dots) \quad (1)$$

with n sufficiently large to remove the optic disc.

On the shade-corrected image we calculate the local variation for each pixel x within a window centered at x . Let $\mathcal{W}(x) \in \mathcal{D}_f$ be the set of pixels within a window centered at x , N the number of pixels in $\mathcal{W}(x) \in \mathcal{D}_f$ and let $\mu_{l_1}(x)$ be the mean value of $l_1(\xi) \quad \forall \quad \xi \in \mathcal{W}(x)$, then we can calculate l_2

$$l_2(x) = \frac{1}{N-1} \cdot \sum_{\xi \in \mathcal{W}(x)} (l_1(\xi) - \mu_{l_1}(x))^2. \quad (2)$$

If k is chosen relatively high and the image l_1 is clipped, we reduce the contrast of exudates more than the contrast of the papillary region because the high contrast of the latter one is partially due to the vessels. The global maximum of l_2 is situated within the papilla or next to it. It allows one to work now on a subimage of the original that contains the optic disc but not large exudates. We note that this approach does not work with mean filters because they do not preserve the borders of image features. Therefore, pixels that do not belong to bright regions but that are close to borders of bright regions are darkened by the shade-correction operator and cause high grey level variation in the shade-corrected image.

Working on the subimage obtained in that way, we can apply a simple area threshold on it—as we know approximately the size of the optic disc—in order to obtain a binary image b , that contains a part of the papilla. Its centroid $c \in \mathcal{D}_f$, that can be calculated as the maximum of the discrete distance function of the biggest particle of b [shown in Fig. 1(b)] can be considered as an approximation for the locus of the optic disc.

3) *Finding the Contours of the Optic Disc Using the Watershed Transformation*: In a first step, we filter the image f_r in order to eliminate large gray level variations within the papillary region. First, we “fill” the vessels, applying a simple closing

$$p_1 = \phi^{(s_1 B)}(f_r) \quad (3)$$

with a hexagonal structuring element $s_1 B$ bigger than the maximal width of vessels. In order to remove large peaks, we open p_1 with a large structuring element. As this alters the shape of the papillary region considerably, we calculate the morphological reconstruction

$$p_2 = R_{p_1}(\gamma^{(s_2 B)}(p_1)). \quad (4)$$

Before we apply the watershed transformation to the morphological gradient $\Delta p_2 = \delta^{(B)} p_2 - \varepsilon^{(B)} p_2$ [shown in Fig. 1(e)], which would lead to oversegmentation of the image, we impose internal and external markers. As internal marker, we use the center c that has been calculated in Section II-D.II, as external marker we use a circle $\mathcal{C}(c)$ with center at c with radius bigger than the diameter of the optic disc [see Fig. 1(d)]

as external marker. We obtain for the marker image m and for the result p_{fin}

$$m(x) = \begin{cases} \Delta p_2, & \text{if } x \in \{c\} \cup \mathcal{C}(c) \\ t_{\max}, & \text{if } x \notin \{c\} \cup \mathcal{C}(c) \end{cases}$$

$$p_{fin} = WS[R_{\Delta p_2}^*(m)] \quad (5)$$

with $WS(f)$ being the watershed transformation of f . This transformation assigns to each local minimum of f one catchment basin (one connected region), in a way that all $x \in \mathcal{D}_f$ belong to a basin except a one pixel strong line that delimits the basins (the so-called watershed line). If we write $p_{fin} = WS[R_{\Delta p_2}^*(m)]$, we mean that $p_{fin}(x) = t_{\max}$ for all pixels within the catchment basin that contains c and 0 elsewhere. Fig. 1(f) shows the result p_{fin} of the segmentation algorithm.

E. Results

We tested the algorithm on 30 color images of size 640×480 that have not been used for the development of the algorithm. The images were taken with a SONY color video 3CCD camera on a Topcon TRC 50 IA retinograph. In 29 images, we could localize the optic disc with the proposed technique. In 27 of 29 images, we also found the exact contours (see, for example, Fig. 2). However, in some of the images, there were small parts missing or small false positives. These shape irregularities in the segmentation result are due to the outgoing vessels or to low contrast (see Fig. 3). We could regularize the shape using standard morphological filter techniques, but the result is still acceptable for our purposes. However, in two images the contrast was too low or the red channel too saturated, the algorithm failed and the result was not acceptable.

III. DETECTION OF EXUDATES

A. Outlines

Hard exudates are yellowish intraretinal deposits, which are usually located in the posterior pole of the fundus. The exudate is made up of serum lipoproteins, thought to leak from the abnormally permeable blood vessels, especially across the walls of leaking microaneurysms. Hard exudates are often seen in either individual streaks or clusters or in large circinate rings surrounding clusters of microaneurysms. They have an affinity for the macula, where they are usually intimately associated with retinal thickening. Hard exudates may be observed in several retinal vascular pathologies, but are a main hallmark of diabetic macular edema. Indeed, diabetic macular edema is the main cause of visual impairment in diabetic patients. It needs to be diagnosed at an early and still asymptomatic stage; at that stage, laser treatment may prevent visual loss from macular edema. Diabetic macular edema is defined by retinal thickening involving or threatening the center of the macula. It is usually diagnosed on slit-lamp biomicroscopy or stereo macular photographs. However, when screening for diabetic retinopathy using a nonmydriatic camera, good macular stereoscopic photographs may be difficult to obtain. In this case, the easiest and most effective way to diagnose macular edema is to detect hard exudates, which are usually associated with macular edema.

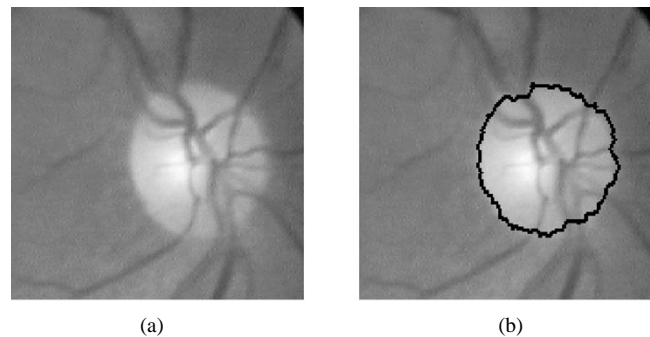


Fig. 2. (a) Luminance channel of the original image. (b) Segmentation result.

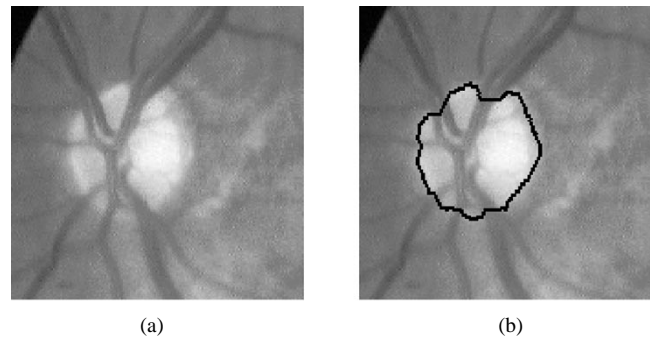


Fig. 3. (a) Luminance channel of the original image. (b) Segmentation result.

Indeed, the presence of hard exudates within $3000 \mu\text{m}$ of the centre of the macula allows macular edema to be detected with a sensitivity of 94%, and a specificity of 54% [25].

B. Properties

As stated in [26], exudates appear as bright patterns in color fundus images of the human retina and they are well contrasted with respect to the background that surrounds them. Their shape and size vary considerably and their borders are mostly irregular [see Figs. 7(a) and 8(a)]. Hard and soft exudates can be distinguished because of their color and the sharpness of their borders.

However, there are a few problems to handle. There are other features in the images that appear as bright patterns, namely the optic disc and—because of changes in illumination—ordinary background pixels. In addition, they are not the only features causing a high local contrast. The grey level variation due to vessels is often as high as the one caused by the exudates.

C. State of the Art

In [13], an algorithm consisting in shade correction, contrast enhancement, sharpening, and a manually chosen threshold is applied to this problem. However, we think that a full automation of exudate detection is possible.

Actually, in [12], a fully automated method based on image sharpening, shade correction, and a combination of local and global thresholding has been proposed and validated.

In [2], color normalization and local contrast enhancement are followed by fuzzy C-means clustering and neural networks are used for the final classification step. This has been shown to work well, but it relies on the local contrast enhancement that has been introduced in [1], and that amplifies noise particularly in areas, in which there are not many features.

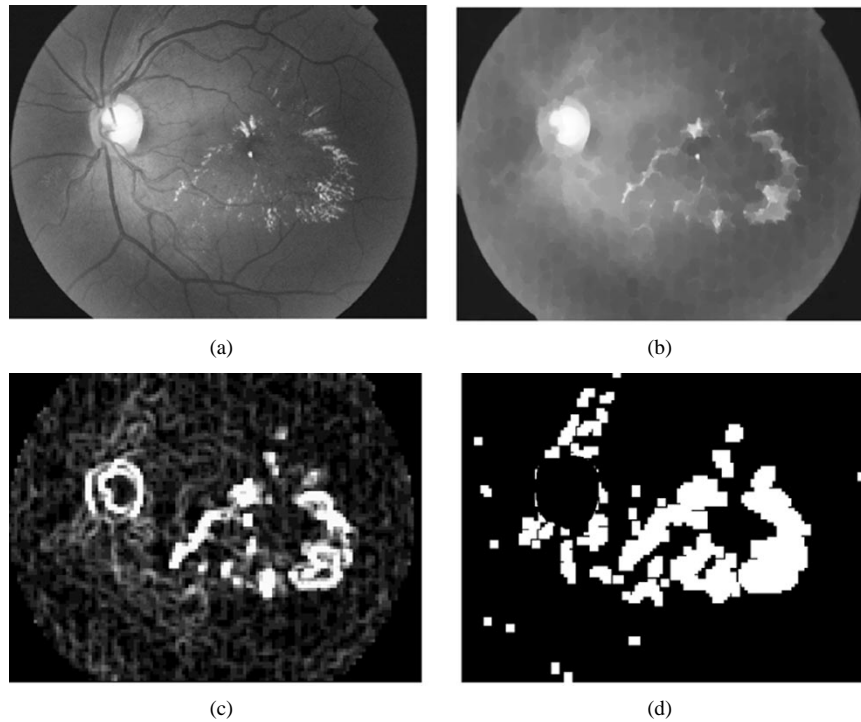


Fig. 4. (a) Luminance channel of a color image of the human retina. (b) Closing of the luminance channel. (c) Local standard variation in a sliding window. (d) Candidate region.

D. Approach Based on Morphological Techniques

As stated in [2], it is the green channel f_g , in which the exudates appear most contrasted. Our algorithm can be divided into two parts. First, we find candidate regions, these are regions that possibly contain exudates. Then, we apply morphological techniques in order to find the exact contours.

1) *Finding of the Candidate Regions:* Regions that contain exudates are characterized by a high contrast and a high grey level. The problem that occurs if we use the local contrast to determine regions that contain exudates, is that bright regions between dark vessels are also characterized by a high local contrast. So, we first eliminate the vessels by a closing [see Fig. 4(b)]

$$e_1 = \phi^{(s_1 B)}(f_g) \quad (6)$$

with s_1 such that $s_1 B$ is larger than the maximal width of the vessels.

On this image, we calculate the local variation for each pixel x within a window $\mathcal{W}(x)$ as in Section II-D.2 [see Fig. 4(c)]

$$e_2(x) = \frac{1}{N-1} \cdot \sum_{\xi \in \mathcal{W}(x)} (e_1(\xi) - \mu_{e_1}(x))^2. \quad (7)$$

Thresholding the image e_2 at grey level α_1 , we obtain all regions with a standard variation larger than or equal to α_1 , i.e., small bright objects and borders of large bright objects. In order to obtain the whole candidate regions rather than their borders, we fill the holes by reconstructing the image from its borders \mathcal{B}_f . We also dilate the candidate region in order to ensure that there are background pixels next to exudates that are included in the candidate regions; this is important for finding the contours

$$e_3 = \delta^{(sB)}(T_{[\alpha_1, t_{\max}]}(e_2))$$

$$e_4 = R_{e_3}^*(b) \quad \text{with} \quad b = \begin{cases} 0, & \text{if } x \in \mathcal{B}_f \\ t_{\max}, & \text{if } x \notin \mathcal{B}_f \end{cases}. \quad (8)$$

The threshold α_1 is chosen in a very tolerant manner, i.e., we get the regions containing some exudates, but we also get some false positives: The papillary region and some other areas that are characterized by a sufficiently high grey level variation due to illumination changes in the image.

Finally, we have to remove the candidate region that results from the optic disc. We remove a dilated version of the segmentation result of Section II. In that way, we obtain as candidate regions [see Fig. 4(d)]

$$e_5 = e_4 - e_4 \wedge \delta^{(sB)}(p_{fin}). \quad (9)$$

2) *Finding the Contours:* In order to find the contours of the exudates and to distinguish them from bright well contrasted regions that are still present in e_5 , we set all the candidate regions to 0 in the original image [see Fig. 5(a)]

$$e_6(x) = \begin{cases} 0, & \text{if } e_5(x) \neq 0 \\ f_g(x), & \text{if } e_5(x) = 0 \end{cases} \quad (10)$$

and we then calculate the morphological reconstruction by dilation of the resulting image under f_g [see Fig. 5(a)]

$$e_7(x) = R_{f_g}(e_6). \quad (11)$$

This operator propagates the values $f_g(x)$ of pixels x next to the candidate regions into the candidate regions by successive geodesic dilation under the mask f_g . As exudates are entirely comprised within the candidate region, they are completely removed, whereas regions that are not entirely comprised in the candidate regions are nearly entirely reconstructed.

The final result [see Figs. 6, 7(b), and 8(b)] is obtained by applying a simple threshold operation to the difference between the original image f_g and the reconstructed image e_7

$$e_{fin} = T_{[\alpha_2, t_{\max}]}(f_g - e_7). \quad (12)$$

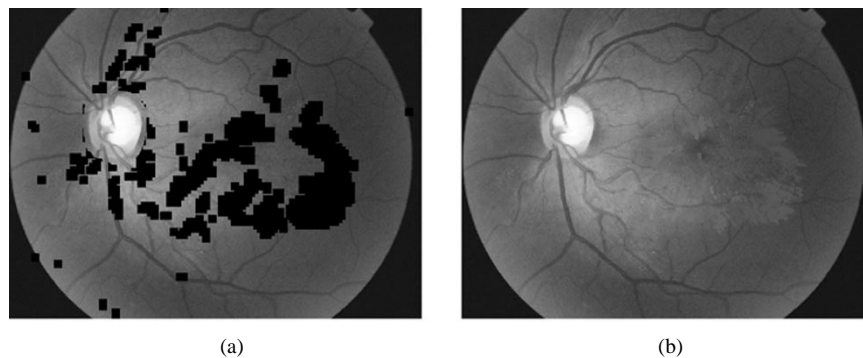


Fig. 5. (a) Candidate regions set to 0 in the original image. (b) Morphological reconstruction.

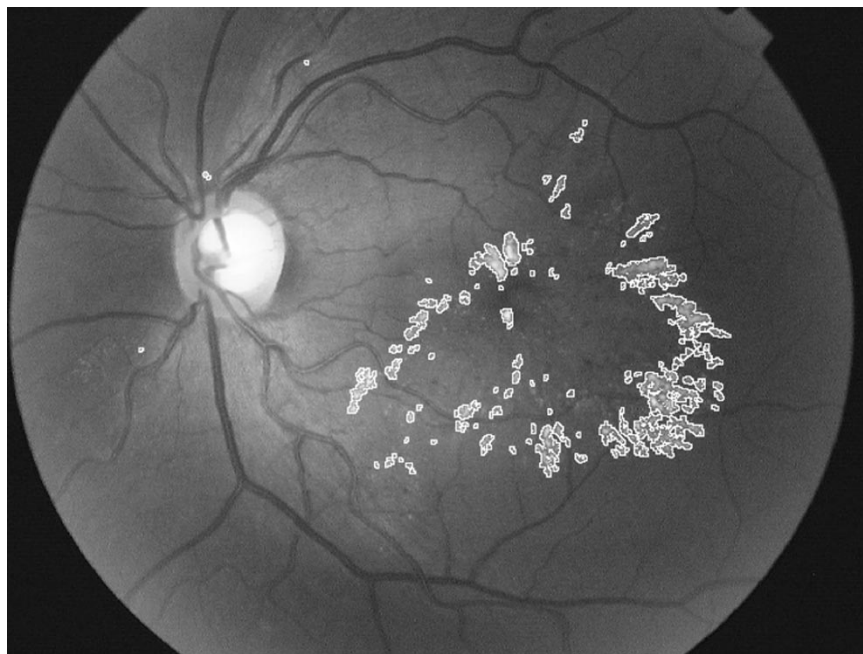


Fig. 6. Result of the segmentation algorithm.

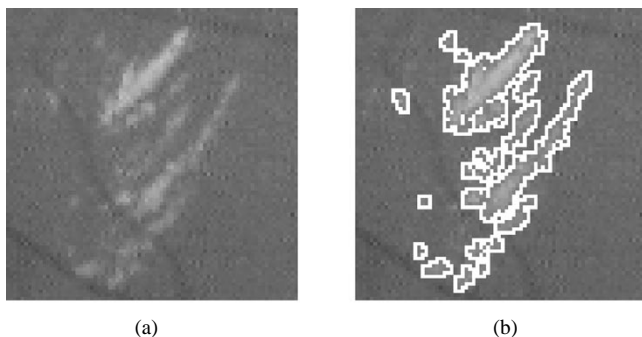


Fig. 7. (a) Detail of the green channel of a color image containing exudates. (b) Segmentation result.

This algorithm has three parameters: the size of the window \mathcal{W} , and the two thresholds α_1 and α_2 . The choice of the size of \mathcal{W} is not crucial, and we have found good results for a window size of 11×11 . However, if the window size is chosen too large, small isolated exudates are not detected. We found that not very disturbing, because small isolated exudates do not play an important role for diagnostic purposes. The first threshold α_1 determines the minimal variation value within the window that is

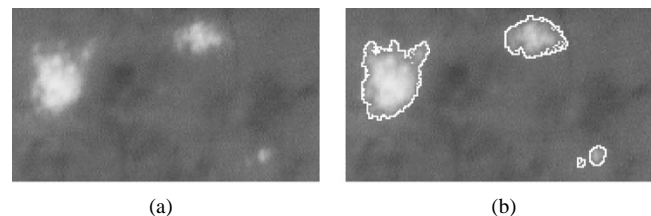


Fig. 8. (a) Detail of the green channel of a color image containing exudates. (b) Segmentation result.

suspected to be a result of the presence of exudates. If α_1 is chosen too low, specificity decreases; if it is set too high, sensitivity decreases. The parameter α_2 is a contrast parameter: It determines the minimal value a candidate must differ from its surrounding background to be classified as an exudate. The influence of these two parameters is discussed in the next section.

E. Results

The assessment of the quality of pathology detection is not an easy task; human graders are not perfect. Hence, if a human grader does not agree with the algorithm, this can be due to an error of the human grader or due to an error of the algorithm.

One more problem arises, if (as for exudates) it has to be defined, when an exudates can be considered as having been detected and when not (pixelwise against objectwise comparison of segmentation results).

In [2], the authors detect candidate objects, that are classified by a human grader and by the neural network as exudates or nonexudates. Comparing these two results allows one to calculate sensitivity and specificity. However, it is not the number of exudates which is important for the diagnosis: If an algorithm can find all exudates, but not the borders in a correct manner, it will have good statistics but poor performance. In [12], a pixelwise comparison is proposed. We shall apply a variant of this method in the next section.

1) *Comparison of the Proposed Method With Human Graders:* We have tested the algorithm on an image data base of 30 images 640×480 digital images taken with a SONY color video 3CCD camera on a Topcon TRC 50 IA retinograph. These images have not been used for the development of the algorithm. 15 of these images did not contain exudates, and in 13 of these 15 no exudates were found by our algorithm. In two images, few false positives were found (less than 20 pixels).

In order to compare the results (for the 15 images containing exudates) obtained by the algorithm with the performance of a human grader, we asked a human specialist to mark the exudates on color images. In that way, we obtained a segmentation result r_1 that we considered to be correct. Then we applied the proposed algorithm and obtained a segmentation result r_2 . Let $\mathcal{S}(f)$ be the support of f defined as the set of pixels for which $f(x) \neq 0$, let $\#S$ be the number of its elements and \setminus the set difference. We define true positives (TPs), false negatives (FNs), and false positives (FPs) in the following way:

$$\begin{aligned} TP &= \# [\mathcal{S}(r_1 \wedge r_2)] \\ FN &= \# [\mathcal{S}(r_1) \setminus \mathcal{S}(r_1 \wedge \delta^B r_2)] \\ FP &= \# [\mathcal{S}(r_2) \setminus \mathcal{S}(\delta^B r_1 \wedge r_2)]. \end{aligned} \quad (13)$$

In the ordinary definition of TP, FN, and FP, the results r_1 r_2 are not dilated. We introduced that in order to make the statistics more robust against small errors on the borders of the segmentation: If a pixel has not been marked by the human grader, but it was marked by the algorithm and it is next to a pixel marked by the human grader, it is not considered as a false positive. However, there we have to note that in that way $FN + TP$ is not the number of pixels classified by the grader as belonging to exudates, and $FP + TP$ is not the number of pixels found by the algorithm as exudate pixels.

Rather than the absolute numbers of pixels, we consider normally sensitivity and specificity that are defined in the following way:

$$\begin{aligned} \text{sensitivity} &= \frac{TP}{TP + FN} \\ \text{specificity} &= \frac{TN}{TN + FP}. \end{aligned} \quad (14)$$

The number of true negatives, i.e., the number of pixels that are not classified as exudate pixels, neither by the grader nor by the algorithm is very high, so the specificity is always near 100%. This is not very meaningful. Therefore, in [12], the absolute of false positives is given. An alternative is to calculate the ratio

TABLE I
COMPARISON OF THE RESULT OF THE SEGMENTATION ALGORITHM WITH THE PERFORMANCE OF A HUMAN GRADER

	TP	FP	FN	sensitivity	pred.value
Image 1	1318	137	39	97.1	90.6
Image 2	3792	136	404	90.3	96.5
Image 3	4188	82	311	93.0	98.1
Image 4	430	12	38	91.9	97.3
Image 5	351	40	31	91.9	89.8
Image 6	1204	106	71	94.4	91.9
Image 7	3758	190	193	95.1	95.2
Image 8	762	66	55	93.3	92.0
Image 9	975	42	103	90.4	95.9
Image 10	520	192	85	86.0	73.0
Image 11	1715	126	71	96.0	93.2
Image 12	2577	245	145	94.7	91.3
Image 13	430	8	71	85.8	98.2
Image 14	1311	163	47	96.5	88.9
Image 15	579	37	32	94.8	94.0

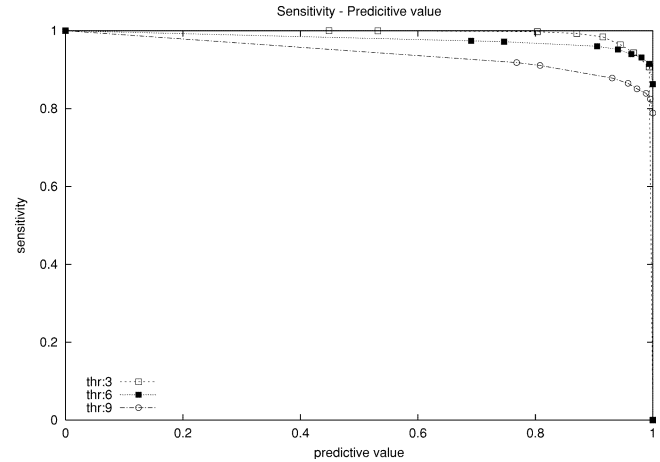


Fig. 9. Sensitivity and the predictive value depending on different parameters.

$TP/(TP + FP)$, that is the probability that a pixel that has been classified as exudate is really an exudate (predictive value).

The results are shown in Table I. We obtain a mean sensitivity of 92.8% and a predictive value of 92.4%.

2) *Influence of the Parameters:* The robustness of an algorithm can be defined in respect to changes in the parameters or to image quality (influence of noise, low contrast, resolution [18]). We have studied the behavior of the algorithm concerning changes of parameters.

In order to study the influence of the parameters α_1 and α_2 , we vary the two parameters within a wide range. We test the algorithm with the following sets of parameters:

- $\alpha_1 \in \{3, 6, 9\}$;
- $\alpha_2 \in \{2, 3, 8, 10, 12, 14, 16, 20\}$.

The results are shown for image 2 in Fig. 9 and for image 3 in Fig. 10. We observe that the segmentation results get worse for $\alpha_1 = 9$, but even in this case we obtain a specificity of over 80% for a predictive value larger than 80% with a good choice of α_2 . Indeed, we can observe that the choice for the parameters is not independent: The lower α_1 , the higher α_2 has to be chosen in

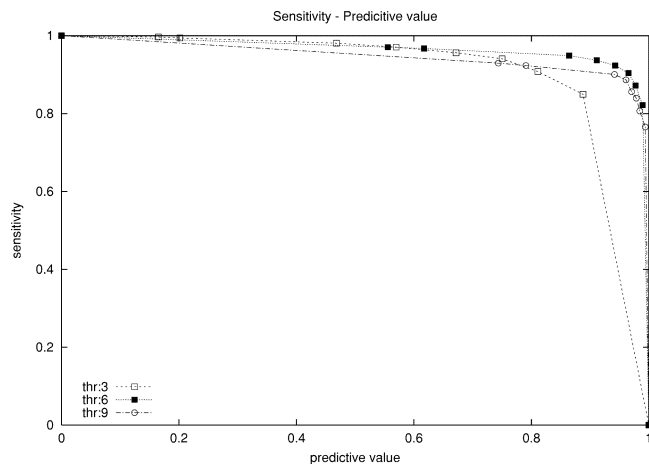


Fig. 10. Sensitivity and the predictive value depending on different parameters.

order to get acceptable results and vice versa. We can state that the behavior of the algorithm with respect to parameter changes is quite robust.

IV. CONCLUSION

Image processing of color fundus images has the potential to play a major role in diagnosis of diabetic retinopathy. There are three different ways in which it can contribute: image enhancement, mass screening (including detection of pathologies and retinal features), and monitoring (including feature detection and registration of retinal images). Efficient algorithms for the detection of the optic disc and retinal exudates have been presented. Robustness and accuracy in comparison to human graders have been evaluated on a small image database. The results are encouraging and a clinical evaluation will be undertaken in order to be able to integrate the presented algorithm in a tool for diagnosis of diabetic retinopathy. Further steps shall be the distinction between hard exudates and soft exudates (cotton wool spots), which is not possible with the proposed algorithm and the evaluation of localization and distribution of the detected exudates in order to detect macular edema.

REFERENCES

- [1] C. Sinthanayothin, J. F. Boyce, H. L. Cook, and T. H. Williamson, "Automated localization of the optic disc, fovea and retinal blood vessels from digital color fundus images," *Br. J. Ophthalmol.*, vol. 83, pp. 231–238, Aug. 1999.
- [2] A. Osareh, M. Mirmehdi, B. Thomas, and R. Markham, "Automatic recognition of exudative maculopathy using fuzzy c-means clustering and neural networks," in *Proc. Medical Image Understanding Analysis Conf.*, July 2001, pp. 49–52.
- [3] M. H. Goldbaum, N. P. Katz, S. Chaudhuri, M. Nelson, and P. Kube, "Digital image processing for ocular fundus images," *Ophthalmol. Clin. North Amer.*, vol. 3, Sept. 1990.
- [4] T. Walter, "Détection de Pathologies Rétiniennes à Partir d'Images Couleur du Fond d'œil," Rapport d'avancement de thèse, Ecole des Mines de Paris, Centre de Morphologie Mathématique, Paris, France, 2000.
- [5] M. J. Cree, J. A. Olson, K. C. McHardy, P. F. Sharp, and J. V. Forrester, "The preprocessing of retinal images for the detection of fluorescein leakage," *Phys. Med. Biol.*, vol. 44, pp. 29–308, 1999.
- [6] E. Peli and T. Peli, "Restoration of retinal images obtained through cataracts," *IEEE Trans. Med. Imag.*, vol. 8, pp. 401–406, Dec. 1989.
- [7] B. Layé, "Analyse Automatique des Images Angiofluorographiques au Cours de la Rétinopathie Diabétique," Ecole Nationale Supérieure des Mines de Paris, Centre de Morphologie Mathématique, Paris, France, 1983.
- [8] T. Spencer, R. P. Phillips, P. F. Sharp, and J. V. Forrester, "Automated detection and quantification of microaneurysms in fluorescein angiograms," *Graefe's Arch. Clin. Exp. Ophthalmol.*, vol. 230, pp. 36–41, 1991.
- [9] A. J. Frame, P. E. Undill, M. J. Cree, J. A. Olson, K. C. McHardy, P. F. Sharp, and J. F. Forrester, "A comparison of computer based classification methods applied to the detection of microaneurysms in ophthalmic fluorescein angiograms," *Comput. Biol. Med.*, vol. 28, pp. 225–238, 1998.
- [10] F. Zana, "Une Approche Morphologique Pour les Détections et Bayésienne Pour le Recalage d'Images Multimodales: Application aux Images Rétiniennes," Ecole Nationale Supérieure des Mines de Paris, Centre de Morphologie Mathématique, Paris, France, 1999.
- [11] S. C. Lee, E. T. Lee, R. M. Kingsley, Y. Wang, D. Russell, R. Klein, and A. Wan, "Comparison of diagnosis of early retinal lesions of diabetic retinopathy between a computer system and human experts," *Graefe's Arch. Clin. Exp. Ophthalmol.*, vol. 119, pp. 509–515, 2001.
- [12] R. Phillips, J. Forrester, and P. Sharp, "Automated detection and quantification of retinal exudates," *Graefe's Arch. Clin. Exp. Ophthalmol.*, vol. 231, pp. 90–94, 1993.
- [13] N. P. Ward, S. Tomlinson, and C. J. Taylor, "Image analysis of fundus photographs – The detection and measurement of exudates associated with diabetic retinopathy," *Ophthalmol.*, vol. 96, pp. 80–86, 1989.
- [14] K. Akita and H. Kuga, "A computer method of understanding ocular fundus images," *Pattern Recogn.*, vol. 15, no. 6, pp. 431–443, 1982.
- [15] S. Tamura and Y. Okamoto, "Zero-crossing interval correction in tracing eye-fundus blood vessels," *Pattern Recogn.*, vol. 21, no. 3, pp. 227–233, 1988.
- [16] S. Chaudhuri, S. Chatterjee, N. Katz, M. Nelson, and M. Goldbaum, "Detection of blood vessels in retinal images using two-dimensional matched filters," *IEEE Trans. Med. Imag.*, vol. 8, pp. 263–269, Sept. 1989.
- [17] A. Pinz, M. Prantl, and P. Datlinger, "Mapping the human retina," *IEEE Trans. Med. Imag.*, vol. 1, pp. 210–215, Jan. 1998.
- [18] F. Z. and J.-C. Klein, "Segmentation of vessel like patterns using mathematical morphology and curvature evaluation," *IEEE Trans. Image Processing*, vol. 10, pp. 1010–1019, July 2001.
- [19] T. Walter and J.-C. Klein, "Segmentation of color fundus images of the human retina: Detection of the optic disc and the vascular tree using morphological techniques," in *Proc. 2nd Int. Symp. Medical Data Analysis (ISMDA 2001)*, Oct. 2001, pp. 282–287.
- [20] F. Mendels, C. Heneghan, and J.-P. Thiran, "Identification of the optic disk boundary in retinal images using active contours," in *Proc. Irish Machine Vision Image Processing Conf. (IMVIP'99)*, Sept. 1999, pp. 103–115.
- [21] F. Z. and J.-C. Klein, "A multi-modal segmentation algorithm of eye fundus images using vessel detection and hough transform," *IEEE Trans. Med. Imag.*, vol. 18, May 1999.
- [22] P. Soille, *Morphological Image Analysis: Principles and Applications*. New York: Springer-Verlag, 1999.
- [23] J. Serra, *Image Analysis and Mathematical Morphology—Theoretical Advances*. London, U.K.: Academic, 1988, vol. 2.
- [24] S. Beucher and F. Meyer, "The morphological approach to image segmentation: The watershed transformation," *Math. Morphology Image Processing*, pp. 433–481, 1993.
- [25] G. H. Bresnick, D. B. Mukamel, J. C. Dickinson, and D. R. Cole, "A screening approach to the surveillance of patients with diabetes for the presence of vision-threatening retinopathy," *Ophthalmol.*, vol. 107, pp. 13–24, 2000.
- [26] P. Massin, A. Erginay, and A. Gaudric, *Rétinopathie Diabétique*. Paris, France: Elsevier, 2000, vol. 1.